Surface hopping dynamics using a locally diabatic formalism: Charge transfer in the ethylene dimer cation and excited state dynamics in the 2-pyridone dimer

Felix Plasser, Giovanni Granucci, Jiri Pittner, Mario Barbatti, Maurizio Persico, and Hans Lischka

Citation: The Journal of Chemical Physics **137**, 22A514 (2012); doi: 10.1063/1.4738960
View online: http://dx.doi.org/10.1063/1.4738960
View Table of Contents: http://scitation.aip.org/content/aip/journal/jcp/137/22?ver=pdfcov
Published by the AIP Publishing

Surface hopping dynamics using a locally diabatic formalism: Charge transfer in the ethylene dimer cation and excited state dynamics in the 2-pyridone dimer

Felix Plasser,[1,a)] Giovanni Granucci,[2] Jiri Pittner,[3] Mario Barbatti,[4] Maurizio Persico,[2] and Hans Lischka[1,5,b)]

[1]*Institute for Theoretical Chemistry, University of Vienna, Waehringergrstrasse 17, A 1090 Vienna, Austria*
[2]*Dipartimento di Chimica e Chimica Industriale, Universita di Pisa, via Risorgimento 35, 56126 Pisa, Italy*
[3]*J. Heyrovský Institute of Physical Chemistry, Academy of Sciences of the Czech Republic, v.v.i., Dolejškova 3, 18223 Prague 8, Czech Republic*
[4]*Max-Planck-Institut für Kohlenforschung, Kaiser-Wilhelm-Platz 1, 45470 Mülheim an der Ruhr, Germany*
[5]*Department of Chemistry and Biochemistry, Texas Tech University, Lubbock, Texas 79409-1061, USA*

(Received 17 May 2012; accepted 9 July 2012; published online 1 August 2012)

In this work, the advantages of a locally diabatic propagation of the electronic wave function in surface hopping dynamics proceeding on adiabatic surfaces are presented providing very stable results even in challenging cases of highly peaked nonadiabatic interactions. The method was applied to the simulation of transport phenomena in the stacked ethylene dimer radical cation and the hydrogen bonded 2-pyridone dimer. Systematic tests showed the reliability of the method, in situations where standard methods relying on an adiabatic propagation of the wave function and explicit calculation of the nonadiabatic coupling terms exhibited significant numerical instabilities. Investigations of the ethylene dimer radical cation with an intermolecular distance of 7.0 Å provided a quantitative description of diabatic charge trapping. For the 2-pyidone dimer, a complex dynamics was obtained: a very fast (<10 fs) initial S_2/S_1 internal conversion; subsequent excitation energy transfers with a characteristic time of 207 fs; and the occurrence of proton coupled electron transfer (PCET) in 26% of the trajectories. The computed characteristic excitation energy transfer time of 207 fs is in satisfactory agreement with the experimental value of 318 fs derived from the vibronic exciton splittings in a monodeuterated 2-pyridone dimer complex. The importance of nonadiabatic coupling for the PCET related to the electron transfer was demonstrated by the dynamics simulations. © *2012 American Institute of Physics*. [http://dx.doi.org/10.1063/1.4738960]

I. INTRODUCTION

Ultrafast dynamical processes play an important role in many fields of chemistry, physics, and molecular biology such as in the photophysics of biomolecules and defect transport in organic semiconductors.[1] These processes are often governed by nonadiabatic couplings between electronic and nuclear degrees of freedom, presenting a special challenge in their simulation. Several computational strategies have been introduced for this purpose (cf., e.g., Refs. 2 and 3): wave packet methods;[4,5] trajectory based simulations;[6,7] and global models[2,8] building on the concepts of Fermi's golden rule, Marcus and Förster theory.[9] From these methods trajectory surface hopping has gained significant popularity because of its conceptual simplicity, ease of interpretation and due to the fact that all molecular degrees of freedom can be included without prior assumptions regarding active modes.[6,10–14] In this contribution, a particular focus will be laid on the application of surface hopping to charge and energy transport phenomena (cf. Refs. 14–16). Such calculations impose special challenges as the transport process is represented by interactions between several states located on different fragments and frequent state crossings. Especially systems with weak interchromophore coupling (for example, because of large spatial separation) may be difficult to describe accurately. In this case, a very low physical transfer probability has to go along with a high hopping probability between the adiabatic states (cf. Ref. 16). It is, of course, highly desirable that the general surface hopping approaches described above are able to treat the dynamics for any interchromophore coupling strength properly.

To illustrate the potential problems, in Figure 1, a model of an avoided crossing in a nuclear displacement coordinate ξ is presented. The adiabatic energies are computed by diagonalizing the model Hamiltonian

$$\mathbf{H}(\xi) = \begin{pmatrix} \left(\xi - \frac{1}{2}\right)^2 & c \\ c & \left(\xi + \frac{1}{2}\right)^2 \end{pmatrix} \quad (1)$$

for different values of a constant diabatic coupling c. The nonadiabatic coupling in the ξ coordinate follows from the derivative of the mixing angle with respect to the nuclear displacement coordinate ξ (cf. Refs. 4, 16, and 17). It forms a peak in the crossing region. As c is lowered (light grey lines), the adiabatic states start to approach each other more closely and at the same time, the coupling becomes increasingly peaked. Note that the area below the coupling

a)Electronic mail: felix.plasser@univie.ac.at.
b)Electronic mail: hans.lischka@univie.ac.at.

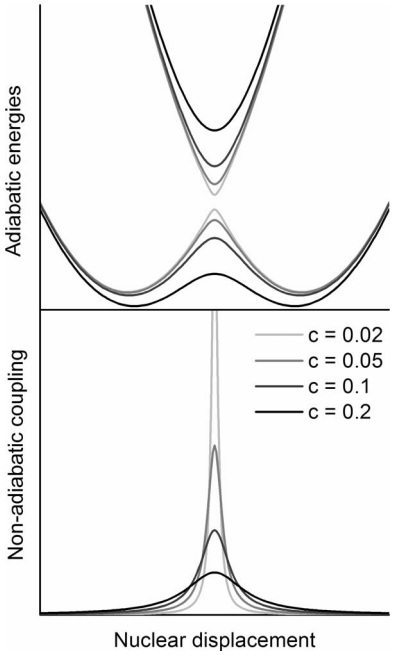

FIG. 1. Model for an avoided crossing at different coupling strengths c (see the text for a description of the formula used). The adiabatic energies of the two states involved, as well as the nonadiabatic coupling between them is shown.

curve always remains constant at $\pi/2$, and therefore, an increase of the peak height occurs together with the narrowing of the peak. In the limit of $c = 0$, which means that an intersection between the two energy curves occurs, the coupling becomes a δ-function. For numerical results and a more detailed discussion of the underlying equations, consider, e.g., Refs. 4 and 16. The extremely narrow shape of the nonadiabatic coupling clearly presents a numerical challenge for using it for the propagation of the electronic wave function. In fact the problem is split into two parts[7] related to the sampling and interpolating of the coupling vector, as well as a numerically accurate propagation of the electronic coefficients. In particular, it should be pointed out that a mere reduction of the timestep length used in the process of propagating the electronic coefficients is not sufficient if the interaction terms are not represented correctly. But an accurate sampling of the nonadiabatic terms may necessitate an increase in the number of electronic structure calculations, which means that in some cases the computational effort for dynamics simulations may be enlarged by an order of magnitude or more (see also Ref. 18). In this contribution, it will be shown that these problems can be overcome by using a locally diabatic representation of the electronic states, which contains only smoothly varying quantities (whereas the nuclear motion still proceeds on adiabatic surfaces).[10] The method is tested here for transfer processes, but it may provide significant improvements also in other situations where highly peaked nonadiabatic interactions are present and, as a consequence, conversion probabilities between diabatic states are low. The case of spin-forbidden transitions, as an example of this phenomenon, is discussed in Ref. 19 contained in this Special Issue.

As an initial step results obtained from an analytic model will be presented. Then two interesting problems will be used

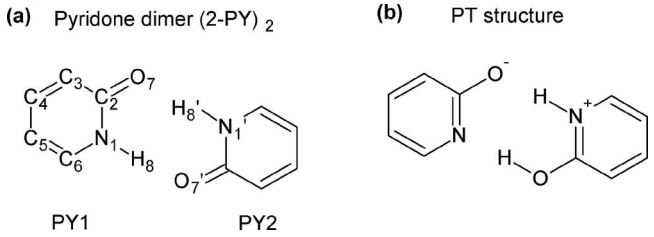

FIG. 2. Structural representation and numbering scheme of the 2-pyridone dimer (a) and the zwitterionic structure present after a single proton transfer (b).

to test and apply the local diabatization method. First, charge transport in the stacked ethylene dimer radical cation [Et.-Et.]$^+$ will be considered. This system serves as an important model system, where the main features of charge transport can be studied. This work will be concerned, in particular, with the weakly coupled case present at an intermolecular separation of 7.0 Å. In our previous study, using the standard Tully surface hopping method in an adiabatic basis with utilizing nonadiabatic coupling vectors, it was not possible to properly treat this case due to highly peaked nonadiabatic coupling vectors.[16] This challenging situation will be revisited here and used as a benchmark case for the different methods of integrating the electronic wave function. The second example is concerned with the 2-pyridone dimer $(2\text{-PY})_2$ (Figure 2(a)). This system can be seen as a model DNA base pair where both, the processes of energy transfer as well as a potential proton coupled electron transfer (PCET) can be studied.[20,21] However, compared to DNA bases this system is significantly simpler, making it a suitable target for experimental and theoretical investigations.

II. METHODS

A. Propagation of the electronic wave function

In the surface hopping approach,[6,22] nuclear motion is treated by classical dynamics according to forces coming from an electronic structure calculation. Interactions between the states are treated through stochastic hoppings between the surfaces. The total time-dependent wave function $\Psi(\mathbf{R},t)$ at time t (nuclear coordinates $\mathbf{R}$ are written explicitly here, electronic coordinates are implicitly considered in the matrix elements), is written as a time-dependent linear combination of N_s adiabatic electronic eigenstates $\varphi_i(\mathbf{R}(t))$,

$$\Psi(\mathbf{R},t) = \sum_{i=1}^{N_s} c_i(t)\,\phi_i(\mathbf{R}(t)) \tag{2}$$

and the coefficients are propagated according to[6]

$$\frac{\mathrm{d}}{\mathrm{dt}} c_j(t) = -\mathrm{i}\,\hbar^{-1} c_j(t)\,E_j(t) - \sum_{i=1}^{N_s} c_i(t)\,\sigma_{ji}(t), \tag{3}$$

where E_j(t) is the energy of the jth adiabatic state. The nonadiabatic interaction matrix element is given as

$$\sigma_{ji}(t) = \left\langle \phi_j(\mathbf{R}(t)) \left| \frac{\partial}{\partial \mathrm{t}} \right| \phi_i(\mathbf{R}(t)) \right\rangle. \tag{4}$$

Traditionally, σ_{ij} is evaluated in terms of the nonadiabatic coupling vector

$$\sigma_{ji}(t) = \dot{\mathbf{R}}(t) \cdot \langle \phi_j(\mathbf{R}) | \nabla | \phi_i(\mathbf{R}) \rangle_{\mathbf{R}=\mathbf{R}(t)}, \tag{5}$$

where ∇ denotes the vector of all first derivatives with respect to the nuclear coordinates. Using Eq. (5) in connection with Eq. (3), will be called "NAC" in the following text. Alternatively, the overlaps of the wave functions between two successive timesteps

$$\mathrm{S}_{ji}(t) = \langle \phi_j(\mathbf{R}(t-\Delta t)) | \phi_i(\mathbf{R}(t)) \rangle \tag{6}$$

may be used.[13,23–25] The coupling can be estimated from linear extrapolation as

$$\sigma_{ji}(t) \approx \frac{1}{4\Delta t}(3\mathrm{S}_{ji}(t) - 3\mathrm{S}_{ij}(t) - \mathrm{S}_{ji}(t-\Delta t) + \mathrm{S}_{ij}(t-\Delta t)). \tag{7}$$

Inserting this into Eq. (3), corresponds to a scheme where wave function overlaps are used in a linear extrapolation formalism (OVL).[23,25] The difficulty in both the NAC and OVL schemes is that, as explained above, close to conical intersections the σ_{ij} are highly peaked and electronic structure calculations have to be performed with a very small timestep Δt to accurately sample this peak. The problem can be overcome by using a different propagation technique where the Hamiltonian matrix between two time steps is interpolated in a locally diabatic basis.[10] At the beginning of each timestep the locally diabatic functions $\eta_i(t)$ are set equal to the adiabatic functions

$$\eta_i(t) = \phi_i(t). \tag{8}$$

The row vector $\{\eta_i(t+\Delta t)\}$ defining the locally diabatic functions at the end of the timestep is constructed according to

$$\{\eta_i(t+\Delta t)\} = \{\phi_i(t+\Delta t)\}\mathbf{T}^{-1}, \tag{9}$$

where the transformation matrix $\mathbf{T}$ is constructed by a Löwdin orthogonalization[26] of the $\mathbf{S}(t+\Delta t)$ matrix (Eq. (6)). Using $\mathbf{T}$, the diabatic Hamiltonian $\mathbf{H}$ at timestep $(t+\Delta t)$,

$$\mathbf{H}(t+\Delta t) = \mathbf{T}\mathbf{E}(t+\Delta t)\mathbf{T}^{-1}, \tag{10}$$

is computed by transforming the diagonal matrix containing the adiabatic energies $\mathbf{E}(t+\Delta t)$. Through this construction, the dynamic couplings (σ_{ij}) in the locally diabatic basis should become negligible (as far as the coupling with the states φ_i, $i > N_s$ can be neglected) and are replaced in Eq. (3) by the smoothly varying matrix elements H_{ij}. Then the coefficient vector $\mathbf{c}(t)$ can be easily propagated in the diabatic basis and finally back transformed to the adiabatic basis

$$\mathbf{c}(t+\Delta t) = \mathbf{T}^{-1}\exp\left(-\mathrm{i}\,\hbar^{-1}\frac{\mathbf{E}(t)+\mathbf{H}(t+\Delta t)}{2}\Delta t\right)\mathbf{c}(t). \tag{11}$$

In summary, local diabatization (LD) provides a way of propagating the wave function without explicit reference to the dynamic couplings (σ_{ij}) and it will be shown that especially in cases where these are highly peaked, LD provides a significantly more stable integration, than the NAC and OVL algorithms discussed above. It should be noted here that the LD formalism only affects the electronic amplitudes and possible state switches, but the nuclei are propagated on the adiabatic potential surfaces just like in the other methods. In particular, if there are no state switches, all three methods produce identical nuclear trajectories.

B. Analysis of charge transfer dynamics

The microscopic properties of the charge transfer dynamics are analyzed as outlined in Ref. 16 to allow for a statistical summary of the dynamics and a comparison with the underlying ideas of Marcus theory. The first quantity considered is the probability of an adiabatic charge transfer per single passage through the transition region. It is reformulated from the Landau-Zener (LZ) probability as[27]

$$P_{12} = 1 - \exp\left(\frac{-\left(H_{if}^{\mathrm{diab}}\right)^2}{\mathrm{h}\nu}\sqrt{\frac{\pi^3}{\lambda \mathrm{k} T}}\right), \tag{12}$$

where H_{if}^{diab} is the diabatic coupling, ν is the harmonic frequency of the active vibration, λ is the reorganization energy, T is the absolute temperature, and h and k are the Planck and Boltzmann constants, respectively. If, after starting in the ground state, this adiabatic transfer failed, the system will continue in the excited state. In the excited state relaxation process, there is an additional chance for a charge transfer and hence the global electronic transmission factor is larger than P_{12}. It is given as[16,27]

$$\kappa_{\mathrm{el}} = \frac{2P_{12}}{1+P_{12}}. \tag{13}$$

C. Phenomenological analysis of excited states

For the analysis of the excited states, we use a recently developed method, which is based on the one electron transition density matrix,[28] cf. also Ref. 29. This method provides well defined, automatized descriptors for properties like the position, delocalization, and charge transfer character of the wave function even in difficult cases (e.g., delocalized orbitals, many contributing configurations). First, charge transfer numbers for an excited state are computed

$$\Omega_{AB} = \frac{1}{2}\sum_{\substack{a\in A\\ b\in B}}(\mathbf{D}^{[\mathrm{AO}]}\mathbf{S}^{[\mathrm{AO}]})_{ab}(\mathbf{S}^{[\mathrm{AO}]}\mathbf{D}^{[\mathrm{AO}]})_{ab} \tag{14}$$

from the transition density matrix between this state and the ground state $\mathbf{D}^{[\mathrm{AO}]}$ and the overlap matrix $\mathbf{S}^{[\mathrm{AO}]}$, both expressed in the atomic orbital (AO) basis. The summations go over the basis functions on fragments A and B, respectively. Using the charge transfer numbers (Eq. (14)), the position of the exciton in the dimer can be defined as

$$POS = \frac{3}{2} + \frac{\Omega_{22}-\Omega_{11}}{2\Omega}, \tag{15}$$

where the symbol Ω is used to represent the normalization factor

$$\Omega = \Omega_{11} + \Omega_{12} + \Omega_{21} + \Omega_{22}. \tag{16}$$

From Eq. (15), it can be seen that *POS* is equal to one and two, for states localized on monomer one ($\Omega_{11} = \Omega$) and monomer two ($\Omega_{22} = \Omega$), respectively. For excitonic delocalized states ($\Omega_{11} = \Omega_{22} = \Omega/2$) and charge separated states ($\Omega_{11} = \Omega_{22}$

$= 0$), $POS = 3/2$. The excitonic delocalization may be defined as a participation ratio expression (cf. Ref. 30)

$$PR = \frac{\Omega^2}{2}\left(\frac{1}{\sum_A \left(\sum_B \Omega_{AB}\right)^2} + \frac{1}{\sum_B \left(\sum_A \Omega_{AB}\right)^2}\right), \tag{17}$$

where the summation goes over the two molecules ($A = 1,2$; $B = 1,2$). For localized ($\Omega_{11} = \Omega$ or $\Omega_{22} = \Omega$) and directed charge transfer states ($\Omega_{12} = \Omega$ or $\Omega_{21} = \Omega$) this measure amounts to one. For excitonic delocalized states ($\Omega_{11} = \Omega_{22} = \Omega/2$) or charge resonance states ($\Omega_{12} = \Omega_{21} = \Omega/2$) or a combination of these two types $PR = 2$. Whereas the *POS* and *PR* values were used to describe the position and delocalization of the exciton, electron transfer was monitored by fragment charge differences (FCD) computed from Mulliken populations.[31]

III. COMPUTATIONAL DETAILS

The charge transfer dynamics in the ethylene dimer radical cation [Et.-Et.]$^+$ was performed in accordance with the investigations reported in Ref. 16: A symmetric face-to-face arrangement of [Et.-Et.]$^+$ was constructed using intermolecular separations of 5.0 Å and 7.0 Å. Surface hopping dynamics simulations were performed at the state-averaged complete active space self-consistent field (CASSCF) level with three electrons in the two π and two π^* orbitals of the two molecules and with state averaging over the two lowest doublet states (SA(2)-CASSCF(3/4)). The 6-311+G* basis set was used.[32] In a first testing stage short trajectories of about 20 fs simulation time, which exhibited one passage through the crossing region, were considered. Five initial conditions each were chosen for [Et.-Et.]$^+$ at the 5.0 Å and 7.0 Å intermolecular separations and all three methods (NAC, OVL, LD) with different time step lengths were tested. This amounted to 75 simulation runs in total. In order to observe the primary mixing between the adiabatic states and to exclude stochastic features, no surface hoppings were allowed and no decoherence correction was applied in these test runs. For a statistical analysis, the following quantities were considered. The mean of a set of similar trajectories was computed as

$$\mu(\Delta t, M) = \frac{1}{N}\sum_{k=1}^{N} c^{(k)}_{\Delta t, M}, \tag{18}$$

where $c^{(k)}_{\Delta t, M}$ denotes the adiabatic population of the ground state after one passage through the crossing region for initial condition k (i.e., c is used as a short notation for $c_0(t_{\mathrm{ref}})$ of Eq. (2)), timestep length Δt and method M ($M =$ NAC, OVL, LD). Additionally, the mean absolute error for a timestep length Δt and method M was computed as

$$\varepsilon(\Delta t, M) = \frac{1}{N}\sum_{k=1}^{N} \left| c^{(k)}_{\Delta t, M} - c^{(k)}_{\mathrm{ref}} \right|. \tag{19}$$

The reference was chosen as the average between the results of using nonadiabatic coupling vectors and local diabatization for the smallest timestep considered (Δt_{min}),

$$c^{(k)}_{\mathrm{ref}} = \frac{c^{(k)}_{\Delta t_{\mathrm{min}},\mathrm{NAC}} + c^{(k)}_{\Delta t_{\mathrm{min}},\mathrm{LD}}}{2}, \tag{20}$$

where the Δt_{min} was 0.2 fs in the case of an intermolecular separation of 5.0 Å, and 0.1 fs in the case of 7.0 Å.

After testing the methods, a production run of 49 surface hopping trajectories with 1 ps duration and a timestep of 0.5 fs was performed using the LD method. A decoherence correction with a decay parameter of 0.1 Hartree was applied,[33] noting that this is particularly important because of the small diabatic coupling[34] and because of the fact that the system passed through the crossing region for several times during each trajectory simulation.[35] As in Ref. 16, a restraining potential was applied to fix the relative arrangement of the molecules.

Following Ref. 21, calculations on the 2-pyridone dimer were performed using time-dependent density functional theory (TDDFT) (Refs. 36 and 37) with the BHLYP functional containing 50% Hartree-Fock exchange.[38] The SVP basis set[39] with added diffuse functions (SVP+sp) (Ref. 40) was used. First, test runs using the OVL and LD methods were performed. Aside from the timestep lengths (Δt), two parameters affecting the duration of CI-overlap computations significantly had to be tested, the screening threshold β_{max} (the maximal value of the CI coefficient function β_{IJ} in Eq. (15) of Ref. 25, for which the corresponding overlap term is still computed) and the number of orbitals treated as a frozen core (n_{core}). For the final dynamics simulations, the LD method with $\Delta t = 0.5$ fs, $\beta_{\mathrm{max}} = 1 \times 10^{-4}$, $n_{\mathrm{core}} = 38$ was used. When using these thresholds reliable nonadiabatic interactions can be obtained (as shown below) at only a fraction of the computational time of the TDDFT energy and gradient calculation. Three excited states were considered in the dynamics. The initial conditions were constructed from the Wigner distribution of the harmonic vibrational ground state of the hydrogen bonded dimer (cf. Ref. 12). Using this construction, the total energy during the dynamics corresponds to the sum of the potential energy of the initial excited state at the sampled molecular geometry and the independently sampled initial kinetic energy. The initial state of the dynamics was chosen randomly according to the relative oscillator strengths of the first two excited states. This amounted to 100 trajectories started from the S_2 state and 33 from the S_1 state. The trajectories were run for 300 fs. When computing the time-dependent state distribution (see below), special attention was paid to trajectories, which could not successfully be run for 300 fs, a situation which occurred in many cases because after PCET the S_1/S_0 gap approached zero. In such a case, the state of the last successful time step was taken for the remaining time steps. Considering that wavefunctions are not available within TDDFT, overlaps were computed from the TDDFT response functions, which have the same formal structure as configuration interaction with single excitations (CIS),[36] a procedure, which has also been used successfully by several other authors.[13,24,41]

In $(2\text{-PY})_2$, proton transfer was monitored by means of interatomic distances. A proton transfer was considered if the N_1-H_8 (N_1'-H_8') distance was longer than the H_8-O_7' (H_8'-O_7) distance (Figure 2). In the dynamics, a proton transfer process was counted if this situation lasted for at least 2 fs. Charge and excitation energy transfer processes were analyzed following the lines described in Ref. 16: Charge (excitation energy) transfer in [Et.-Et.]$^+$ ($(2\text{-PY})_2$) was monitored by using

the FCD (*POS* value). A charge (excitation energy) transfer from molecule one to molecule two was registered if initially for at least 3 fs the dimer was in the D_0 (S_1) state and the FCD (*POS* value) was smaller than −0.5 (1.05), and later on, for at least 3 fs, the dimer would be again in the D_0 (S_1) state, but now with a FCD (*POS* value) greater than 0.5 (1.95). The transfer from molecule two to molecule one was defined in an analogous fashion.

The excited state analysis described in Sec. II C was carried out using the transition densities of the formal CIS wavefunctions[36] which were computed for the wavefunction overlaps as described above. Fragment charge differences[31] between the two molecules were computed from the Mulliken populations. In the case of proton transfers, the fragments were adjusted to reflect the movement of the proton.

An analysis in terms of normal mode displacements, as described in Ref. 42 was performed as well. For each trajectory k and time t, the Cartesian difference vector $\mathbf{x}(k,t)$ between that structure and the ground state reference geometry ($\mathbf{x}_0$) was converted to $\mathbf{y}(k,t)$ in the normal mode basis by the relation

$$\mathbf{y}(k,t) = \mathbf{V}^{-1}(\mathbf{x}(k,t) - \mathbf{x}_0), \tag{21}$$

where $\mathbf{V}^{-1}$ is the transformation matrix from Cartesian to normal coordinates computed at $\mathbf{x}_0$. For all non-totally symmetric modes the absolute value of the displacement was taken since motions into both directions are equivalent. To characterize the $\mathbf{y}(k,t)$ vectors, they were first averaged over all trajectories and second the standard deviation over time of this time-dependent average was computed.

The SA-CASSCF calculations were performed with the COLUMBUS 7.0 program package.[43] The TDDFT computations were carried out using TURBOMOLE.[37,44] For the dynamics simulations and wavefunction overlap computations the NEWTON-X program package[12,25,41,45] was used.

IV. RESULTS AND DISCUSSION

A. Model system

Before proceeding to simulations of molecular systems, the performance of the three integration formalisms NAC, OVL, and LD was tested with respect to the LZ model for an avoided crossing. A one-dimensional time-dependent diabatic model Hamiltonian between two states was defined according to

$$\mathbf{H}(t) = \begin{pmatrix} 0 & c \\ c & s\xi(t) \end{pmatrix}, \tag{22}$$

$$\xi(t) = v(t - t_0), \tag{23}$$

where the diabatic coupling c, the slope s, and the velocity v are assumed to be constant. Under these assumptions the LZ asymptotic expression for the diabatic transition probability

$$P_{12} = 1 - \exp\left(-\frac{4\pi^2 c^2}{h\,|sv|}\right) \tag{24}$$

is exact. The nonadiabatic coupling between the adiabatic functions $h(\xi)$ has a Lorentzian shape with a full width at half maximum of $|4c/s|$. In analogy, the characteristic time τ to pass through the crossing region can be defined as

$$\tau = \left|\frac{4c}{sv}\right|. \tag{25}$$

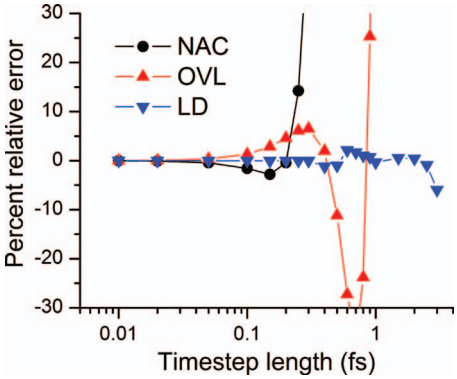

FIG. 3. Landau-Zener model system: relative error for the asymptotic diabatic transition probability as a function of the integration timestep. Presented results are for the three algorithms NAC, OVL, and LD as described in the main text.

In the model calculations, the values $c = 0.0033$, $s = 0.66$, and $v = 0.002$ (all data in atomic units) were chosen. This corresponds to $P_{12} \approx 0.0505$ and $\tau = 20$ a.u. (about 0.48 fs). An integration of this model using the NAC, OVL, and LD using different timestep lengths Δt was performed. In each case, an average over 10 calculations was performed using different crossing times t_0 according to

$$\begin{matrix} t_0 = \Delta t\left(n + \frac{k}{10}\right) \\ k = 0, \ldots, 9 \end{matrix}, \tag{26}$$

where the integer n was chosen such that $vn\Delta t$, the distance traveled before reaching the crossing, was about 5 a.u. With this construction, trajectories with $k = 0$ directly reached the diabatic crossing point, whereas the others sampled points around it. The integrations were started at $t = 0$ assigning a probability of one to one of the two adiabatic states and ended at $t = 200$ fs. The final probability of the adiabatic state initially populated was then identified with P_{12}. In Figure 3, the relative error of this value with respect to the exact LZ value of P_{12} is shown. For short timesteps ($\Delta t \ll \tau$) all three methods give good results. When Δt approaches τ, the results of NAC and OVL diverge. By contrast LD shows impressive stability up to $\Delta t \approx 4\tau$, which is a case where the whole region of non-negligible nonadiabatic interaction is passed within only a fraction of the timestep.

In summary, the fundamental stability of the LD method in the case of highly peaked nonadiabatic interactions between two states could be shown. It should however be noted that, as opposed to NAC, the LD and OVL formalisms are potentially subject to inaccuracies coming from the interactions with "external" states (i.e., the states φ_i with $i > N_s$), which were not included in this test.

B. Ethylene dimer radical cation

The first system considered was the ethylene dimer radical cation, which serves as a convenient model for charge

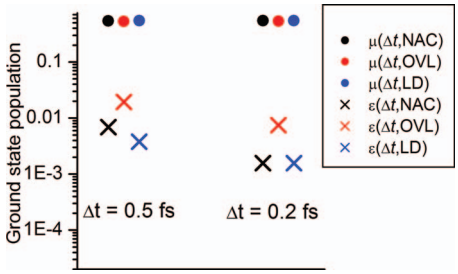

FIG. 4. Mean values μ and mean absolute errors ε of the ground state population after one passage through the crossing region for the ethylene dimer radical cation at an intermolecular separation of 5.0 Å, considering integration timesteps (Δt) of 0.5 and 0.2 fs and using different integration methods.

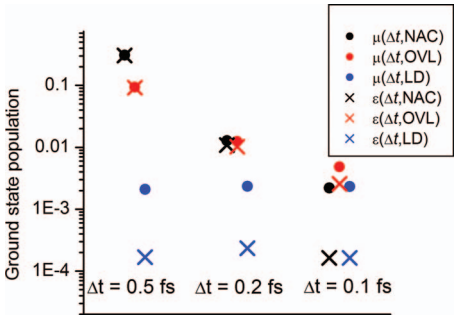

FIG. 5. Mean values μ and mean absolute errors ε of the ground state population after one passage through the crossing region for the ethylene dimer radical cation at an intermolecular separation of 7.0 Å, considering integration timesteps (Δt) of 0.5, 0.2, and 0.1 fs and using different integration methods.

transport in stacked π-systems. The complex was considered with intermolecular separations of 5.0 and 7.0 Å, which corresponds to intermediate and weak coupling situations, respectively. In an initial step, a test of the available methods for integration of the electronic Schrödinger equation was performed. For this purpose, an analysis of dynamics runs with about 20 fs duration containing one passage through the crossing region was carried out. The quantity of interest was the ground state population at the end of the dynamics. The mean $\mu(\Delta t,M)$ (Eq. (18)) and mean absolute error $\varepsilon(\Delta t,M)$ (Eq. (19)) over five different initial conditions were computed for different timestep lengths Δt and the three methods described above M = NAC, OVL, LD.

For an intermolecular separation of 5.0 Å, the diabatic coupling is 0.079 eV, leading to an extended region of weak nonadiabatic coupling (cf. Figure 1, $c = 0.2$).[16] The mean values $\mu(\Delta t,M)$ of the ground state population after one passage through the crossing region are presented in Figure 4. On average, slightly more than half the population remained in the ground state. For NAC and LD, there was a very good agreement with the value of 0.544 within $\pm$ 0.002 for both timestep lengths, whereas for OVL slightly smaller values of 0.527 for $\Delta t = 0.5$ fs, and 0.538 for $\Delta t = 0.2$ fs were found. In all cases, the mean absolute errors $\varepsilon(\Delta t,M)$ with respect to the average of NAC and LD at $\Delta t = 0.2$ fs (cf. Sec. III) were about two orders of magnitude smaller than the mean population transfer, meaning that all methods provide a stable integration for this system. The largest error, at 4% of the total population transfer, was found for OVL ($\Delta t = 0.5$ fs). In summary, it can be said that all methods perform satisfactory, but that NAC and LD seem to be somewhat superior to OVL.

Second, the probability of charge transfer in the ethylene dimer radical cation was computed at an intermolecular separation of 7.0 Å (Figure 5). With a diabatic coupling of only 0.0042 eV this is an example of a weak coupling region of electron transfer.[16] The shape of the nonadiabatic coupling relates to $c = 0.02$ in Figure 1. In practice, the coupling vector was so highly peaked that with $\Delta t = 0.5$ fs for most trajectories there was only one time step with significant nonadiabatic coupling when passing through the crossing region. Considering Sec. IV A, this corresponds to the case of $\tau \approx 0.5$ fs, meaning that NAC and OVL should require significantly smaller timesteps for reliable results. In the calculation with $\Delta t = 0.5$ fs, NAC provides an average charge transfer probability of 0.307 because the numerical integration of the electronic Schrödinger equation clearly missed the peak of the nonadiabatic coupling in some of the trajectories. The charge transfer probability is overestimated by two orders of magnitude compared to the value for $\Delta t = 0.1$ fs. OVL performs somewhat better at the longest timestep length ($\mu = 0.094$) but is still quite far from the result obtained at a smaller timestep length. LD provides very stable values, ($\mu = 0.002$) for all timestep lengths considered. At $\Delta t = 0.1$ fs, the LD value almost coincides with NAC, whereas OVL yields an average transfer probability of about twice as much ($\mu = 0.005$). Here, LD clearly yields the most stable integration algorithm and the results show impressive consistency over the different timestep lengths. A dynamics simulation using the NAC method and $\Delta t = 0.1$ fs could be reliable as well but this would correspond to a five-fold increase in computation time.

After the above considerations, we chose LD ($\Delta t = 0.5$ fs) as the method to perform more extended dynamics simulations on $[\text{Et.-Et.}]^+$ for an intramolecular separation of 7.0 Å. These simulations provide an extension to Ref. 16, where dynamics at 3.0 Å (strong coupling region) and 5.0 Å (intermediate coupling region) were performed. The weak coupling case of 7.0 Å, which had to be omitted because no satisfactory method of integrating the coefficients was available at that time, will be considered now. A representative 300 fs section of the dynamics of this system is shown in Figure 6. For the first 100 fs, the trajectory remains around one of the minima in the double well potential. The FCD always stays very close to one, representing a complete localization of the charge. The energy gap oscillates and in three instances the system moves close to the crossing region (represented by a small energy gap) but does not cross the transition state. The first crossing appears after about 100 fs. However, the charge is not transferred and a diabatic trapping situation is obtained through two consecutive surface hoppings (this corresponds to Scheme 3(b) in Ref. 16). It may be noted here that in regions surrounding nonadiabatic events, some apparent discontinuities are present. However, these are only related to the discrete and stochastic nature of the dynamics, and a change in FCD lasting for only one or two time steps cannot be counted as a charge transfer (cf. Sec. III for the

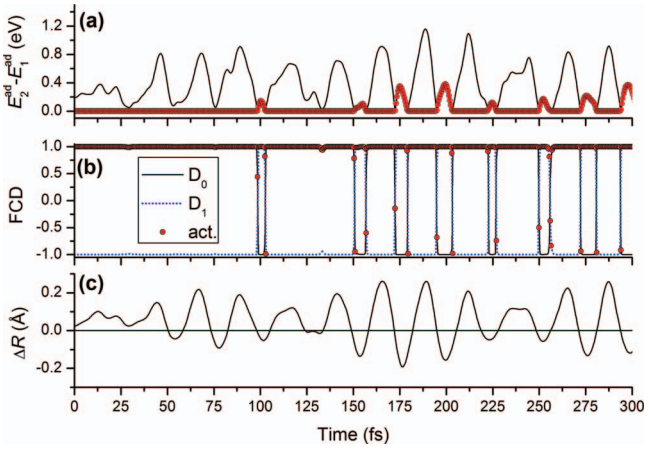

FIG. 6. Energy gap (a) (red circles on the upper line indicate that the system is in the excited state), fragment charge difference (FCD) (b), and CC bond alternation ΔR (c) plotted against time for a [Et.-Et.]$^+$ trajectory with an intermolecular separation of 7.0 Å.

precise algorithm used to identify CT events). For the remaining trajectory, more such events occur. But there is no actual transfer of charge.

In Table I, the electronic transmission factor κ_{el} is given for the intermolecular distance of 7.0 Å in [Et.-Et.]$^+$ derived from LD dynamics simulations for 49 trajectories. For comparison the dynamics simulations of Ref. 16 for [Et.-Et.]$^+$ at an intermolecular separation of 5.0 Å, as well as simulations of this system with an inserted formaldehyde molecule [Et.-FA-Et.]$^+$ are presented. The cases investigated before were situated in the intermediate coupling region with an electronic transmission factor of about 50%. In contrast the [Et.-Et.]$^+$ complex at 7.0 Å, intermolecular distance is clearly a weak coupling case ($\kappa_{el} \approx 1\%$), which corresponds to an electron transfer rate of 0.16 ps^{-1}. The agreement with the Marcus theory type model (Eqs. (12) and (13)) is excellent. Out of 842 accesses to the transition state in the different trajectories, only 8 led to a charge transfer. The diabatic trapping was realized by 1964 surface hoppings in the simulations. In summary, it could be seen that the LD approach was able to filter spurious charge migration events quantitatively.

C. 2-pyridone dimer

The hydrogen bonded 2-pyridone dimer (2-PY)$_2$ has been considered as a model DNA base pair. Two interesting processes, which are also relevant to DNA can be studied: excitation energy transfer between the molecules as well as a possible proton coupled electron transfer, which may lead to non-radiative decay.[20,21] The electronic coupling between the two $\pi\pi^*$ states in (2-PY)$_2$ was estimated at about 0.05 eV from CIS transition moments[20] or 0.07 eV from TDDFT dimer splitting calculations.[21] The experimentally observed splitting was smaller by one order of magnitude at about 0.003 eV.[20] However, it should be noted that the latter is the coupling between vibronic states which is obtained as the product between the electronic coupling and a Franck-Condon factor[20,46] and it is clearly possible that this Franck-Condon factor, representing the overlap between the ground state vibrations in the two equivalent strongly symmetry broken S_1 minima, is only on the order of 5%. In the further course of this discussion, it should be remembered that our simulations were performed in a basis of electronic eigenfunctions, whereas the experimental interpretation is more readily performed using vibronic eigenstates. An attempt to reconcile the two representations will be performed where applicable.

TABLE I. Electronic transmission factors (κ_{el}) for [Et.-Et.]$^+$ with intermolecular distances of $R_{C\ldots C} = 5.0$ Å and $R_{C\ldots C} = 7.0$ Å, and [Et.-FA-Et.]$^+$ with $R_{C\ldots C} = 7.0$ Å.

	[Et.-Et.]$^+$ (5.0 Å)[a]	[Et.-FA-Et.]$^+$[a]	[Et.-Et.]$^+$ (7.0 Å)
Simulation	0.671	0.401	0.010
Model[b]	0.891	0.471	0.010

[a]Results from Ref. 16.
[b]Equation (13) in the text.

The dynamics simulations were performed with the TDDFT/BHLYP method. The reliability of this approach was tested for all tautomers by comparison with second order approximate coupled cluster calculations (CC2).[21] It can, therefore, be assumed that this approach should provide a good description in particular of the EET dynamics. Describing the PCET process is more challenging because charge transfer transitions play a significant role and because of the fact that in the subsequent dynamics the S_1/S_0 gap is significantly lowered. Moreover, complex nonadiabatic effects may come into play.[47] However, interesting qualitative insight may be obtained from these calculations. Moreover, direct dynamics simulations can provide important complementary information with respect to the quite involved global models applied for describing PCET processes.[47]

Before the actual dynamics simulation was started, the effects of the parameters of the overlap computation were explored. This was necessary to assure a stable integration of the electronic coefficients while still operating at an acceptable computational cost. The timestep length Δt, as well as two parameters affecting the performance of the overlap computation were considered (cf. Sec. III). A collection of results considering different values of these parameters for five distinct initial conditions and integration with the OVL and LD methods is presented in Table II. First, it can be observed that in the OVL approach there are some instabilities as far as both the timestep length as well as the parameters of the CI-overlap computation are concerned. In contrast to that, LD yields remarkably stable results, in particular for the initial conditions denoted $k = 1$–4. The stability of LD with respect to timestep length is probably related to the favorable treatment of highly peaked nonadiabatic interactions, as discussed above. The fact that also highly screened overlap matrices are correctly interpreted by LD may be attributed to the fact that in the Löwdin orthogonalization procedure yielding the **T** matrix the screened terms are recovered through a proper renormalization. In the last case ($k = 5$), a particularly challenging example was chosen where in a process with two different nonadiabatic interactions, the population of S_2 was equally distributed between S_1 and S_3. In this case, some small

TABLE II. Population of the S_2 state after a nonadiabatic event for five different initial conditions k, computed using different parameters in the integration process.[a]

Method	Δt (fs)	β_{max}[b]	n_{core}[c]	$c_{\Delta t, M}^{(k)}$ $k=1$	$k=2$	$k=3$	$k=4$	$k=5$
OVL	0.5	5×10^{-3}	38	0.1022	0.223	0.359	0.1242	0.0719
OVL	0.5	1×10^{-4}	38	0.0584	0.178	0.302	0.1024	0.0822
OVL	0.5	1×10^{-4}	28	0.0702	0.193	0.318	0.1095	0.0791
OVL	0.5	5×10^{-5}	28	0.0598	0.179	0.303	0.1041	0.0815
OVL	0.5	1×10^{-5}	0	0.0514	0.167	0.291	0.0992	0.0834
OVL	0.2	5×10^{-5}	0	0.0420	0.167	0.299	0.0600	0.0673
OVL	0.1	5×10^{-5}	0	0.0340	0.164	0.297	0.0535	0.0656
LD	0.5	5×10^{-3}	38	0.0143	0.141	0.271	0.0403	0.0938
LD	0.5	1×10^{-4}	38	0.0147	0.140	0.270	0.0407	0.0852
LD	0.5	1×10^{-4}	28	0.0147	0.140	0.270	0.0413	0.0861
LD	0.5	5×10^{-5}	28	0.0150	0.140	0.269	0.0413	0.0846
LD	0.5	1×10^{-5}	0	0.0150	0.140	0.270	0.0416	0.0829
LD	0.2	5×10^{-5}	0	0.0148	0.138	0.268	0.0443	0.0725
LD	0.1	5×10^{-5}	0	0.0148	0.138	0.268	0.0443	0.0721

[a]The trajectories were started in the S_2 state. In the dynamics two excited states were considered for $k = 1,2,3$; three for $k = 4$; and four for $k = 5$.
[b]Screening threshold according to Eq. (15) of Ref. 25.
[c]Number of core orbitals frozen in the overlap.

variations in the S_2 population are present also within the LD approach. Another point to consider is that even at the smallest timestep no quantitative agreement between OVL and LD could be reached. The computation of analytic TDDFT nonadiabatic coupling vectors has been reported[48] but not implemented in the program systems available to us. Therefore, this discrepancy could not be evaluated further. In any case, there is good qualitative agreement between the two approaches. In particular, it is noted that the LD method using $\Delta t = 0.5$ fs, $\beta_{max} = 1 \times 10^{-4}$, $n_{core} = 38$ provides reliable results. This parameter set is used in the subsequent dynamics simulations.

First, two trajectories will be presented in detail to illustrate the possible processes occurring. Data for a trajectory where the pyridine dimer remains in the initial tautomeric form is presented in Figure 7, whereas in Figure 8 a case that undergoes PCET is shown. Such a process was previously postulated from both TDDFT and CC2 calculations.[21]

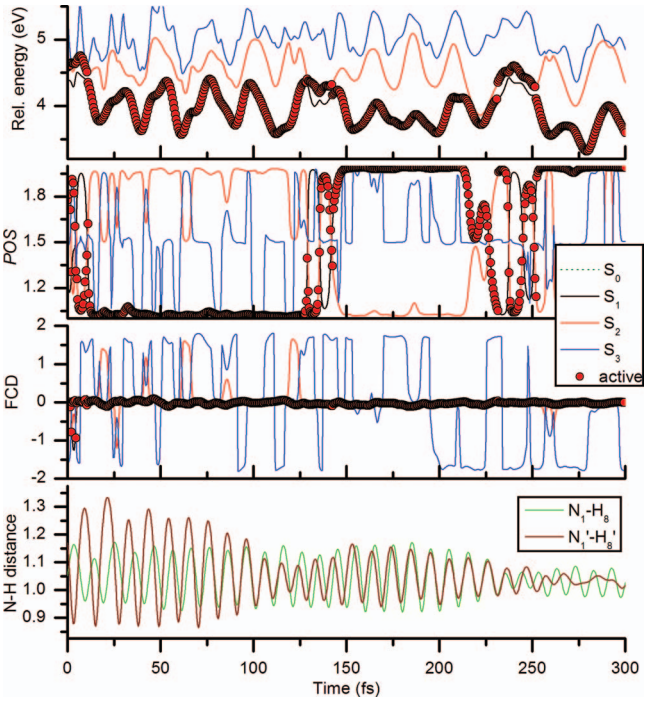

FIG. 7. Relative energies, *POS* values, fragment charge differences (FCD) for the lowest four singlet states (the active state is marked with red circles) and N–H bond lengths of a trajectory of the 2-pyridone dimer, which remains in the initial tautomeric form.

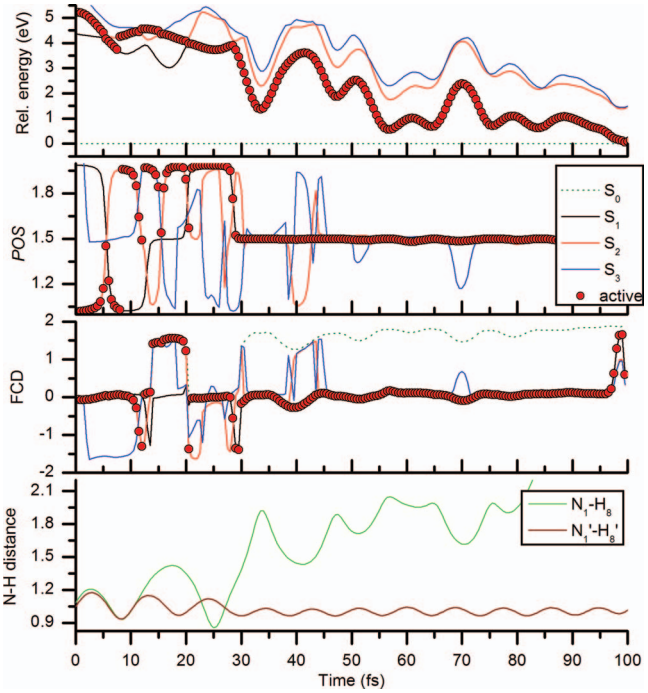

FIG. 8. Relative energies, *POS* values, fragment charge differences (FCD) for the lowest four singlet states (the active state is marked with red circles) and N–H bond lengths of a trajectory of the 2-pyridone dimer, which undergoes a proton coupled electron transfer.

In these plots, a detailed description of the different electronic states is shown: relative energies with respect to the ground state at the respective geometry; *POS* values representing EET; and the fragment charge differences representing charge transfer. Moreover, N–H bond distances are presented to monitor a possible proton transfer. Both trajectories are started in the S_2 state. Figure 7 shows that the early dynamics is determined by a hopping to the S_3 state at 2.0 fs and back to S_2 at 4.5 fs. An analysis of the FCDs reveals that this event is determined by a crossing in diabatic character (S_2 temporarily gains the charge transfer character of S_3), and that this corresponds to a diabatic trapping situation, avoiding charge transfer. A short time after that, at 11.0 fs, a decay to S_1 occurs and the exciton is subsequently localized on PY1 ($POS \approx 1.0$). The exciton remains on PY1 until about 125 fs when a transfer two PY2 occurs. This transfer is characterized by staying a short time in S_2: a hopping to S_2 occurs at 129.0 fs; EET (a change in the *POS* value from one to two) occurs in this state at about 135.5 fs; relaxation to S_1 and trapping of the exciton on PY2 occurs at 142.5 fs (this type of transfer process was explained in more detail in Scheme 3(c) of Ref. 16). During the process just described, there are some additional discontinuities and short time intervals of partial electronic delocalization. These are related to the fact that in Figure 7 the *POS* value of the active adiabatic state of the surface hopping dynamics is plotted, which is only a stochastic representation of the true wave packet. By contrast, the *POS* value of the coherent electronic wavefunction (Eq. (2)) should be a more smoothly varying quantity, representing the transfer process in a more balanced fashion. Around 235 fs there is another nonadiabatic event including a hopping to the S_2 state. However, after relaxation to the S_1 state the exciton is again localized on PY2, i.e., in summary this event does not correspond to a transfer of excitation energy.

For comparison, a trajectory undergoing proton coupled electron transfer is analyzed as well (Figure 8). Such a process represents 26% of our trajectories. The trajectory is started in the S_2 state with $POS = 1.0$. In the initial phase of the dynamics, there is a hopping to S_1 after 5.5 fs and a backhopping to S_2 after 8.0 fs. At 12.0 fs a hopping to S_3 occurs, which is probably related to the diabatic crossing of the *POS* values. Shortly after that (14.0 fs), a proton transfer from PY1 to PY2 occurs (i.e., the H_8 atom is now closer to O_7' than to N_1). After such an event, one can differentiate between two kinds of electronic states: (i) zwitterionic states where only the proton is transferred and the fragments are thus charged and (ii) biradical states where also an electron is transferred leading to an odd number of electrons on either fragment (see also Ref. 21). These two types of states can be identified by their FCDs, which reveal in this case that the S_0, S_2, and S_3 states are of zwitterionic nature, whereas S_1 has a biradical character. The active state after proton transfer is first S_3 then S_2. The diabatic character remains as a zwitterionic state with an excitation on PY2 (the molecule with the extra proton). A back proton transfer along the hydrogen bond, which had remained intact, occurs at 20 fs with a concurrent hopping into S_1. At the next period of the N_1-H_8 vibration another proton transfer occurs at 30 fs. This time the system remains in the S_1 state, which obtains a biradical character. Thus in summary a proton and an electron were transferred from PY1 to PY2, and charge neutrality between the fragments was obtained. However, it should be noted that during this process the S_1 state probability was temporarily reduced to 34% and in one timestep a high hopping probability to S_2 of 74% was obtained. This means that also in this case there was a high likelihood for a diabatic electron trapping. After this proton coupled electron transfer, the structure is strongly stabilized and the N_1-H_8 hydrogen bond broken, significantly reducing the chance for a back transfer. Considering the FCD values, it can be seen that the ground state (dotted line) possesses zwitterionic nature, whereas the three excited states considered are all of biradical nature, i.e., these are reached by charge transfer transitions from the ground state. In the subsequent course of the dynamics the S_1/S_0 energy gap is significantly lowered. In agreement with the CC2 calculations of Ref. 21, we find that an ultrafast internal conversion after the PCET is likely to occur. However, a precise computation of decay times cannot be performed as the reliability of our approach in connection with the PCET process is not certain (as far as the description of the charge transfer transitions as well as of the S_1/S_0 intersection is concerned).

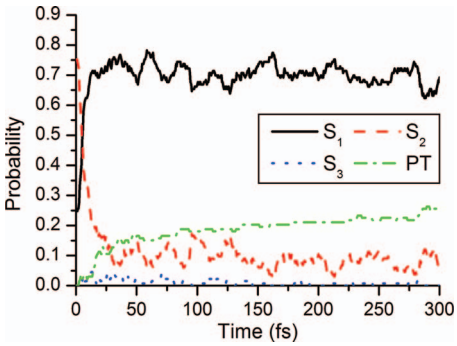

FIG. 9. Development of the state distribution during the 300 fs after photoexcitation in the 2-pyridone dimer. S_1, S_2, and S_3 mark the respective state of the initial tautomer, whereas PT corresponds to the structure where one proton is transferred.

Having thus presented the underlying processes, the general evolution of the dynamics will be discussed. In Figure 9, the S_1, S_2, S_3 populations of the initial $(2\text{-PY})_2$ tautomer, as well as the population of the proton transfer (PT) structure is shown (cf. Figure 2). At $t = 0$ fs, the populations of S_1 and S_2 are 25% and 75%, respectively, according to their ratio in oscillator strengths. The early dynamics is characterized by an ultrafast decay from S_2 to S_1 and already after 5.0 fs these states exhibit equal population. In the subsequent dynamics the population of S_2 is equilibrated at about 8% due to a dynamical process consisting of short recrossings to this state, as shown, for example, in Figure 7 around 135 fs and 235 fs. This dynamical mixing of the S_2 and S_1 states in the semi-classical dynamics can be seen as the corresponding phenomenon to vibronic mixing between these states, as reported from experiment.[20] During the whole course of the dynamics, also a slight involvement of the S_3 state is present. Whereas this value never exceeds a few percent, preliminary tests indicated that including this state is decisive for an accurate description of the dynamics, where it appears to be in

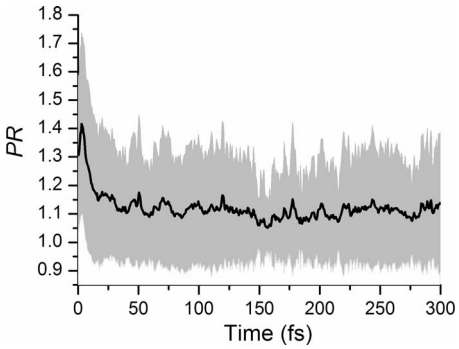

FIG. 10. Development of the excitonic participation ratio (*PR*) during the 300 fs after photoexcitation in the 2-pyridone dimer. The average (black line) as well as the standard deviation (grey area) are shown.

particular important for correctly describing a possible diabatic electron trapping after proton transfer (for example, Figure 8 around 15 fs). Ultrafast PCET is seen as well in these simulations, leading to a biradical excited state of the PT structure (Figure 2(b)). This process is characterized by an initial sharp rise (after 50 fs already 17% of the trajectories are in this structure) and a subsequent significant slowdown (18% after 100 fs; 21% after 200 fs; and 26% after 300 fs).

Another interesting property of the dynamics is the excitonic delocalization, represented by the *PR* value (Eq. (17)). This value is one for localized or (directed) charge transfer states and two for completely delocalized states. The average development of this quantity is presented in Figure 10. The initial average value (± the sample standard deviation over the different trajectories), corresponding to the Franck-Condon excitation lies at $PR = 1.31 \pm 0.28$. Then a brief initial small spike follows as the trajectories relax into the symmetric S_2 minimum, reaching a maximum of $PR = 1.42 \pm 0.32$ at 3.0 fs. Subsequently, due to switching into the S_1 state, the wavefunction quickly localizes after less than 50 fs reaching an equilibrium of about $PR \approx 1.1$.

To represent the molecular motions in more detail, we perform an analysis of coherent normal mode motions, as explained in Sec. III. A summary of the lower frequency modes up to 1067 cm^{-1} is presented in Figure 11. The most prominent motions are the two totally symmetric intermolecular modes ν_4 (106 cm^{-1}, "shearing") and ν_6 (166 cm^{-1}, "stretching"). Three more totally symmetric modes show significant activity: two in-plane ring deformation modes ν_{15} (581 cm^{-1}) and ν_{26} (896 cm^{-1}); and the C-H in plane bending mode ν_{35} (1067 cm^{-1}). The strong activity of the intermolecular in-plane mode ν_5 (108 cm^{-1}, "opening") of B_u symmetry reflects the symmetry breaking in the dynamics, which yields the localized exciton. This mode is also strongly displaced in the case of proton transfers. It is interesting to compare these results to experiment. Whereas quantum mechanical effects of the nuclear vibrations are not included in our simulations, our results can still be set in qualitative relation to optical spectra, in the sense that it is just the Franck-Condon active modes, which should show coherent motion after excitation. The two intermolecular low energy modes ν_4 and ν_6 were also observed most prominently in two-color resonant two-photon ionization spectra, and activity of ν_5 was reported as

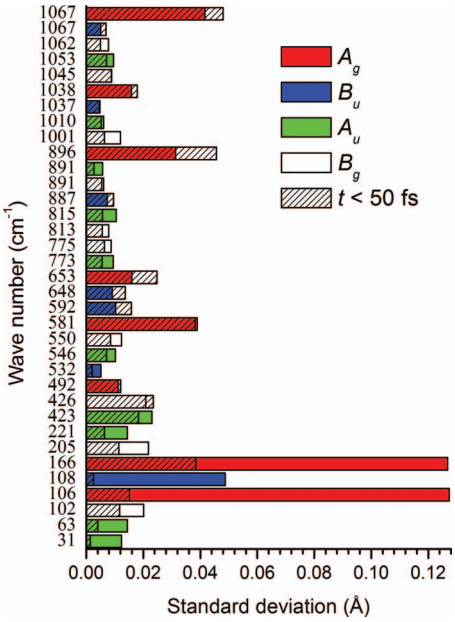

FIG. 11. Coherent normal mode activity during the dynamics as measured by the standard deviation of the averaged displacement vectors with respect to the ground state equilibrium structure. Modes and wave numbers of the ground state equilibrium structure are considered. Color coding is according to the symmetry of the mode; diagonal lines mark activity occurring within the first 50 fs. In-plane modes belong to the A_g and B_u symmetries, out-of-plane modes to A_u and B_g.

well.[20] In dispersed fluorescence experiments, also activity of the modes denoted here ν_{15} and ν_{26} was reported.[20] In summary, it can be seen that the semi-classical dynamics exhibit similar normal mode activity as the experimental absorption and emission spectra. In Figure 12, the time dependence of the normal mode motions is presented. The shearing mode (Figure 12(a)) exhibits a motion separating the two molecules with a maximum separation at about 200 fs and a backward motion afterwards. Also stretching (Figure 12(b)) starts right after the excitation and proceeds in a coherent way, where the maximum is reached after about 125 fs and backward motion after that. The in-plane deformation mode ν_{15}, which is in particular related to the C_2-C_5 distances on each molecule, shows an initial C_2-C_5 contraction followed by a coherent ringing with a period of about 60 fs.

It is of special interest to discuss the transfer processes in more detail. For an analysis of EET the 99 trajectories, which remained in the initial $(2\text{-PY})_2$ tautomeric form were analyzed. In these cases, 142 EET events occurred in total, leading to a transfer time of 207 fs. An experimental reference for this value of 318 fs was derived from the vibronic exciton splittings in a monodeuterated $(2\text{-PY})_2$ complex.[20] The agreement between these two values is quite good and suggests that the TDDFT/BHLYP approach can describe the process correctly. Moreover, this fact could reconcile the discrepancy regarding excitonic couplings that was pointed out in Ref. 21: Whereas the computed purely electronic couplings are on the order of 0.07 eV, experimental vibronic couplings of 0.003 eV were reported. However, considering the data presented above, it can be seen that when the whole dynamical process is considered, very similar transfer times are obtained in both representations.

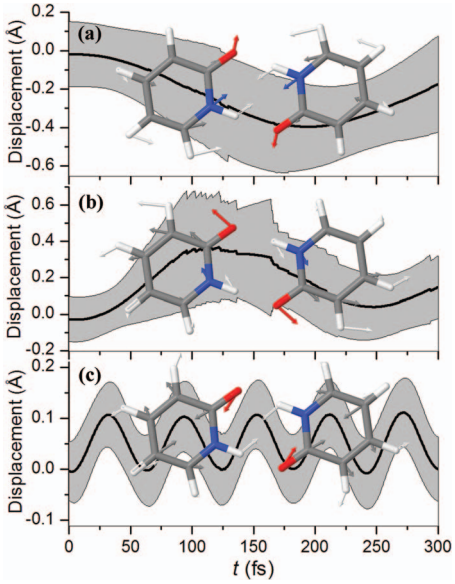

FIG. 12. Time evolution of mean displacements for three selected totally symmetric normal modes: ν_4 (106 cm^{-1}, "shearing") (a), ν_6 (166 cm^{-1}, "stretching") (b), ν_{15} (581 cm^{-1}, in-plane ring deformation) (c). Zero indicates the ground state equilibrium value, positive values indicate a displacement in the direction of the arrows, negative values in the opposite direction. Grey areas indicate ± one standard deviation around the mean.

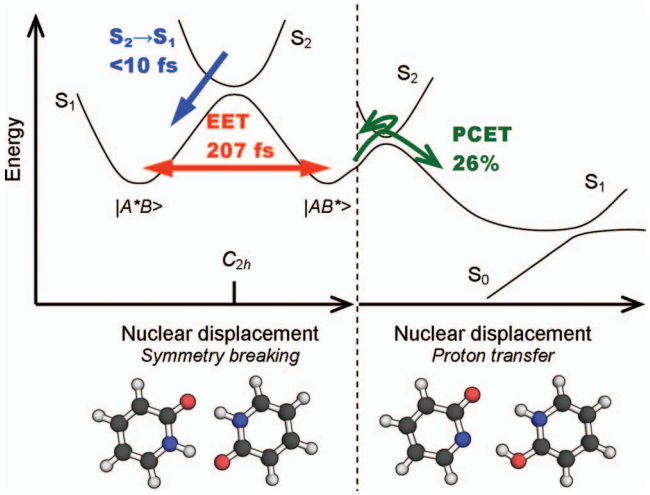

FIG. 13. General scheme of processes occurring in the 2-pyridone dimer after photoexcitation as computed with TDDFT/BHLYP dynamics of 300 fs duration.

In our simulations, a PCET leading to a stabilized PT structure occurred in 26% of the trajectories (cf. Figure 9). These are mostly occurring in the early part of the dynamics. The subsequent slowdown is probably caused by the fact that after excitation the hydrogen bonds are elongated[21] and as presented above (Figures 11 and 12) that major intermolecular motions displace the complex from its initial tightly bound structure. It can, therefore, be assumed that the number of PCET events would not be much larger if the trajectories were run for a longer time. The simulations are therefore consistent with experiment in the sense that a large fraction of the excited complexes does undergo normal fluorescence. The dynamical behavior that went along with these transfers may be of special interest. Aside from PCETs there was a large number of quick back and forth proton transfer events (as shown, for example, in Figure 8 around $t = 15$ fs). These were usually accompanied by surface hoppings, yielding a diabatic trapping of the electron. Therefore, a zwitterionic structure was formed, which quickly stabilized by transferring the proton back. In the 133 trajectories simulated 30 such proton back transfers occurred. This highlights the fact that PCET is a process with significant nonadiabatic interactions and cannot be completely understood when only adiabatic potential energy surfaces are considered.

A summary of the processes occurring after photoexcitation is presented in Figure 13. Internal conversion from S_2 to S_1 occurs within the first 10 fs. Then the symmetry broken S_1 minima are populated. EET between these two equivalent minima occurs on a time scale of 207 fs. Furthermore, we found that PCET may occur, leading to a biradical excited state of the PT structure, which would subsequently relax to an area with a small S_1/S_0 gap. An interesting phenomenon in this context was that in about half of the PT events, a diabatic trapping of the electron involving two consecutive surface hoppings occurred, and a subsequent backwards PT restored the initial tautomer. In spite of this trapping situation, 26% of the trajectories did exhibit PCET in the present simulations.

Finally, possible implications on DNA base pairs will be discussed. EET in $(2\text{-PY})_2$ has been considered as a model for interstrand EET in DNA.[20] In this context, it could be said that the time of 207 fs (experimental value: 318 fs) (Ref. 20) can be seen as a lower bound for the energy transfer time, applicable in the case of two identical molecules and no involvement of environmental degrees of freedom. PCET in DNA is of special interest as it has been considered as a possible decay channel in UV excited DNA base pairs and model systems.[49,50]

In this work, it was observed that in many cases a diabatic trapping of the electron mediated by S_2/S_1 crossings occurred, which lowered the chance of PCET compared to a purely adiabatic treatment. Whereas the PCET itself was observed here, the dynamics after this process, i.e., the possible decay from a biradical S_1 state to the ground state has been examined for a guanine-cytosine Watson-Crick base pair.[50] Also for this situation, a diabatic trapping, realized through S_1/S_0 recrossings, was observed.[50] Thus, in summary it can be concluded that nonadiabatic electron transfer dynamics may play a key role in deciding whether or not a PCET channel is accessible.

V. CONCLUSIONS

The local diabatization method for surface hopping dynamics was investigated with a focus on the simulation of transport phenomena. It was applied to the stacked ethylene dimer radical cation as well as the hydrogen bonded 2-pyridone dimer. Systematic tests using these systems as well as an analytical model showed that this method can provide very stable results even in challenging cases of very fast nonadiabatic events. In contrast, when using nonadiabatic coupling vectors or wave function overlaps with linear extrapolation in

an adiabatic representation of the wave function, significant instabilities were observed when the nonadiabatic interactions were highly peaked. Simulations on the stacked ethylene dimer radical cation with an intermolecular distance of 7.0 Å were performed to represent a case where due to a large spatial separation electron transfer was significantly inhibited. In agreement with the Marcus theory type model, an electronic transmission factor of $\kappa_{el} = 1\%$ was obtained, whereas in the remaining 99% of the barrier crossings a diabatic trapping situation was assured through two consecutive surface hoppings.

In the 2-pyridone dimer, a complex dynamics (see Figure 13 for a summary) was observed including excitation energy transfer as well as the possibility for a proton coupled electron transfer. The trajectories could be characterized by a very fast (<10 fs) initial S_2/S_1 internal conversion. For a subsequent excitation energy transfer between the two localized S_1 minima, a characteristic time of 207 fs was obtained, which is in good agreement with the experimental value of 318 fs.[20] A fraction of 26% of the trajectories exhibited ultrafast proton coupled electron transfer which may subsequently lead to an internal conversion to the ground state. Whether or not this process really plays a decisive role cannot be conclusively answered without more extensive computations or experiments. However, interesting insight into the process could be gained and it could be shown that PCET does not only depend on the adiabatic energy surfaces related to the proton transfer but that also nonadiabatic effects associated with the electron transfer play a crucial role. The implications of these findings on hydrogen bonded DNA base pairs were discussed as well.

ACKNOWLEDGMENTS

F. Plasser is a recipient of a DOC fellowship of the Austrian Academy of Sciences. This work has been supported by the Austrian Science Fund within the framework of the Special Research Program and F41 Vienna Computational Materials Laboratory (ViCoM). This work was also performed as part of research supported by the National Science Foundation Partnership in International Research and Education (PIRE) Grant No. OISE-0730114. Support was also provided by the Robert A. Welch Foundation under Grant No. D-0005. The authors also acknowledge the technical support and computer time at the Vienna Scientific Cluster (Project Nos. 70019 and 70151). J. Pittner acknowledges support by the Granting Agency of the Czech Republic (Project No. 208/12/0559).

[1]C. T. Middleton, K. de La Harpe, C. Su, Y. K. Law, C. E. Crespo-Hernandez, and B. Kohler, Annu. Rev. Phys. Chem. **60**, 217 (2009); M. Barbatti, A. J. A. Aquino, J. J. Szymczak, D. Nachtigallová, P. Hobza, and H. Lischka, Proc. Natl. Acad. Sci. U.S.A. **107**(50), 21453 (2010); F. D. Lewis, H. H. Zhu, P. Daublain, T. Fiebig, M. Raytchev, Q. Wang, and V. Shafirovich, J. Am. Chem. Soc. **128**(3), 791 (2006); J.-L. Brédas, J. E. Norton, J. Cornil, and V. Coropceanu, Acc. Chem. Res. **42**(11), 1691 (2009).
[2]A. F. Izmaylov, D. Mendive-Tapia, M. J. Bearpark, M. A. Robb, J. C. Tully, and M. J. Frisch, J. Chem. Phys. **135**(23), 234106 (2011).
[3]F. Plasser, M. Barbatti, A. J. A. Aquino, and H. Lischka, Theor. Chim. Acta **131**, 1073 (2012).
[4]H. Koppel, W. Domcke, and L. S. Cederbaum, Adv. Chem. Phys. **57**, 59 (1984).
[5]G. A. Worth and L. S. Cederbaum, Annu. Rev. Phys. Chem. **55**, 127 (2004).
[6]J. C. Tully, J. Chem. Phys. **93**(2), 1061 (1990).
[7]B. G. Levine, J. D. Coe, A. M. Virshup, and T. J. Martinez, Chem. Phys. **347**(1-3), 3 (2008).
[8]P. F. Barbara, T. J. Meyer, and M. A. Ratner, J. Phys. Chem. **100**(31), 13148 (1996); G. Scholes, X. Jordanides, and G. Fleming, J. Phys. Chem. B **105**(8), 1640 (2001); D. Abramavicius, B. Palmieri, D. V. Voronine, F. Sanda, and S. Mukamel, Chem. Rev. **109**(6), 2350 (2009).
[9]P. A. M. Dirac, Proc. R. Soc. London, Ser. A **114**(767), 243 (1927); E. Fermi, *Notes on Quantum Mechanics* (University of Chicago, Chicago, IL, 1961); T. Forster, Ann. Phys. **2**(1-2), 55 (1948); R. A. Marcus, Angew. Chem., Int. Ed. Engl. **32**(8), 1111 (1993).
[10]G. Granucci, M. Persico, and A. Toniolo, J. Chem. Phys. **114**(24), 10608 (2001).
[11]N. L. Doltsinis and D. Marx, Phys. Rev. Lett. **88**(16), 166402 (2002); I. Tavernelli, E. Tapavicza, and U. Rothlisberger, THEOCHEM **914**(1-3), 22 (2009); M. Richter, P. Marquetand, J. Gonzalez-Vazquez, I. Sola, and L. Gonzalez, J. Chem. Theory Comput. **7**(5), 1253 (2011); M. Barbatti, R. Shepard, and H. Lischka, in *Conical Intersections: Theory, Computation and Experiment*, edited by W. Domcke, D. R. Yarkony, and H. Köppel (World Scientific, Singapore, 2011), vol. 17.
[12]M. Barbatti, G. Granucci, M. Persico, M. Ruckenbauer, M. Vazdar, M. Eckert-Maksic, and H. Lischka, J. Photochem. Photobiol., A **190**(2-3), 228 (2007).
[13]R. Mitric, U. Werner, and V. Bonacic-Koutecky, J. Chem. Phys. **129**(16), 9 (2008).
[14]T. Nelson, S. Fernandez-Alberti, V. Chernyak, A. E. Roitberg, and S. Tretiak, J. Phys. Chem. B **115**(18), 5402 (2011).
[15]L. Blancafort, P. Hunt, and M. A. Robb, J. Am. Chem. Soc. **127**(10), 3391 (2005).
[16]F. Plasser and H. Lischka, J. Chem. Phys. **134**(3), 034309 (2011).
[17]M. Baer, Phys. Rep. **358**(2), 75 (2002).
[18]T. Nelson, S. Fernandez-Alberti, V. Chernyak, A. E. Roitberg, and S. Tretiak, J. Chem. Phys. **136**(5), 054108 (2012).
[19]G. Granucci, M. Persico, and G. Spighi, J. Chem. Phys. **137**, 22A501 (2012).
[20]A. Muller, F. Talbot, and S. Leutwyler, J. Chem. Phys. **116**(7), 2836 (2002).
[21]E. Sagvolden and F. Furche, J. Phys. Chem. A **114**(25), 6897 (2010).
[22]M. Barbatti, WIREs: Comput. Mol. Sci. **1**, 620 (2011).
[23]S. Hammes-Schiffer and J. C. Tully, J. Chem. Phys. **101**(6), 4657 (1994).
[24]E. Tapavicza, I. Tavernelli, and U. Rothlisberger, Phys. Rev. Lett. **98**(2), 023001 (2007).
[25]J. Pittner, H. Lischka, and M. Barbatti, Chem. Phys. **356**(1-3), 147 (2009).
[26]P. O. Lowdin, J. Chem. Phys. **18**(3), 365 (1950).
[27]B. S. Brunschwig, J. Logan, M. D. Newton, and N. Sutin, J. Am. Chem. Soc. **102**(18), 5798 (1980).
[28]F. Plasser and H. Lischka, "Analysis of excitonic and charge transfer interactions from quantum chemical calculations," J. Chem. Theory Comput. (in press).
[29]A. V. Luzanov and O. A. Zhikol, Int. J. Quantum Chem. **110**(4), 902 (2010); S. Tretiak and S. Mukamel, Chem. Rev. **102**(9), 3171 (2002).
[30]J. Pipek and P. G. Mezey, Int. J. Quantum Chem. **34**(22), 1 (1988); A. Czader and E. R. Bittner, J. Chem. Phys. **128**(3), 035101 (2008).
[31]A. A. Voityuk and N. Rosch, J. Chem. Phys. **117**(12), 5607 (2002).
[32]R. Krishnan, J. S. Binkley, R. Seeger, and J. A. Pople, J. Chem. Phys. **72**(1), 650 (1980).
[33]G. Granucci and M. Persico, J. Chem. Phys. **126**(13), 134114 (2007).
[34]B. R. Landry and J. E. Subotnik, J. Chem. Phys. **135**(19), 191101 (2011).
[35]G. Granucci, M. Persico, and A. Zoccante, J. Chem. Phys. **133**(13), 134111 (2010).
[36]M. Casida, in *Recent Advances in Density Functional Methods, Part I*, edited by D. Chong (World Scientific, Singapore, 1995), p. 155.
[37]R. Bauernschmitt and R. Ahlrichs, Chem. Phys. Lett. **256**(4-5), 454 (1996).
[38]A. Becke, J. Chem. Phys. **98**(7), 5648 (1993); C. Lee, W. Yang, and R. G. Parr, Phys. Rev. B **37**, 785 (1988).
[39]A. Schafer, H. Horn, and R. Ahlrichs, J. Chem. Phys. **97**(4), 2571 (1992).
[40]A. J. A. Aquino, D. Tunega, G. Haberhauer, M. H. Gerzabek, and H. Lischka, J. Phys. Chem. A **106**, 1862 (2002).
[41]M. Barbatti, J. Pittner, M. Pederzoli, U. Werner, R. Mitric, V. Bonacic-Koutecky, and H. Lischka, Chem. Phys. **375**(1), 26 (2010).
[42]F. Plasser, M. Barbatti, A. J. A. Aquino, and H. Lischka, J. Phys. Chem. A **113**(30), 8490 (2009); F. Plasser, M.S. thesis, University of Vienna, 2009.
[43]H. Lischka, R. Shepard, F. B. Brown, and I. Shavitt, Int. J. Quantum Chem.

S15, 91 (1981); H. Lischka, R. Shepard, R. M. Pitzer, I. Shavitt, M. Dallos, T. Muller, P. G. Szalay, M. Seth, G. S. Kedziora, S. Yabushita, and Z. Y. Zhang, Phys. Chem. Chem. Phys. **3**(5), 664 (2001); R. Shepard, H. Lischka, P. G. Szalay, T. Kovar, and M. Ernzerhof, J. Chem. Phys. **96**(3), 2085 (1992); H. Lischka, M. Dallos, and R. Shepard, Mol. Phys. **100**(11), 1647 (2002); H. Lischka, M. Dallos, P. G. Szalay, D. R. Yarkony, and R. Shepard, J. Chem. Phys. **120**(16), 7322 (2004); H. Lischka, R. Shepard, I. Shavitt, R. M. Pitzer, M. Dallos, T. Mueller, P. G. Szalay, F. B. Brown, R. Ahlrichs, H. J. Boehm, A. Chang, D. C. Comeau, R. Gdanitz, H. Dachsel, C. Ehrhardt, M. Ernzerhof, P. Hoechtl, S. Irle, G. Kedziora, T. Kovar, V. Parasuk, M. J. M. Pepper, P. Scharf, H. Schiffer, M. Schindler, M. Schueler, M. Seth, E. A. Stahlberg, J.-G. Zhao, S. Yabushita, Z. Zhang, M. Barbatti, S. Matsika, M. Schuurmann, D. R. Yarkony, S. R. Brozell, E. V. Beck, J.-P. Blaudeau, M. Ruckenbauer, B. Sellner, F. Plasser, and J. J. Szymczak, COLUMBUS, an *ab initio* electronic structure program, release 7.0, 2011, see www.univie.ac.at/columbus; H. Lischka, T. Mueller, P. G. Szalay, I. Shavitt, R. M. Pitzer, and R. Shepard, WIREs: Comput. Mol. Sci. **1**(2), 191 (2011).

[44]R. Ahlrichs, M. Bar, M. Haser, H. Horn, and C. Kolmel, Chem. Phys. Lett. **162**(3), 165 (1989).

[45]M. Barbatti, G. Granucci, M. Ruckenbauer, F. Plasser, J. Pittner, M. Persico, and H. Lischka, NEWTON-X: A package for Newtonian dynamics close to the crossing seam, 2011, see www.newtonx.org.

[46]J. E. Wessel and J. A. Syage, J. Phys. Chem. **94**(2), 737 (1990).

[47]S. Y. Reece and D. G. Nocera, Annu. Rev. Biochem. **78**, 673 (2009).

[48]V. Chernyak and S. Mukamel, J. Chem. Phys. **112**(8), 3572 (2000); C. Hu, H. Hirai, and O. Sugino, *ibid.* **127**(6), 064103 (2007); I. Tavernelli, E. Tapavicza, and U. Rothlisberger, *ibid.* **130**(12), 124107 (2009); R. Send and F. Furche, *ibid.* **132**(4), 044107 (2010).

[49]A. L. Sobolewski, W. Domcke, and C. Hättig, Proc. Natl. Acad. Sci. U.S.A. **102**(50), 17903 (2005); A. Abo-Riziq, L. Grace, E. Nir, M. Kabelac, P. Hobza, and M. de Vries, *ibid.* **102**(1), 20 (2005); T. Schultz, E. Samoylova, W. Radloff, I. V. Hertel, A. L. Sobolewski, and W. Domcke, Science **306**(5702), 1765 (2004).

[50]G. Groenhof, L. V. Schafer, M. Boggio-Pasqua, M. Goette, H. Grubmuller, and M. A. Robb, J. Am. Chem. Soc. **129**(21), 6812 (2007).